Received: 15 November 2020 | Accepted: 27 November 2020

DOI: 10.1002/maco.202012192

ARTICLE

Materials and Corrosion

Preconditioning of AISI 304 stainless steel surfaces in the presence of flavins—Part II: Effect on biofilm formation and microbially influenced corrosion processes

Nina Wurzler[1] | Jan D. Schutter[1] | Ralph Wagner[2] | Matthias Dimper[1] | Vasile-Dan Hodoroaba[1] | Dirk Lützenkirchen-Hecht[2] | Ozlem Ozcan[1]

[1]Bundesanstalt für Materialforschung und -prüfung, Berlin, Germany

[2]Fakultät für Mathematik und Naturwissenschaften—Physik der kondensierten Materie, Bergische Universität Wuppertal, Wuppertal, Germany

Correspondence
Ozlem Ozcan, Bundesanstalt für Materialforschung und -prüfung, 12205 Berlin, Germany.
Email: ozlem.ozcan@bam.de

Abstract

Biofilm formation and microbially influenced corrosion of the iron-reducing microorganism *Shewanella putrefaciens* were investigated on stainless steel surfaces preconditioned in the absence and presence of flavin molecules by means of XANES (X-ray absorption near-edge structure) analysis and electrochemical methods. The results indicate that biofilm formation was promoted on samples preconditioned in electrolytes containing minute amounts of flavins. On the basis of the XANES results, the corrosion processes are controlled by the iron-rich outer layer of the passive film. Biofilm formation resulted in a cathodic shift of the open circuit potential and a protective effect in terms of pitting corrosion. The samples preconditioned in the absence of flavins have shown delayed pitting and the samples preconditioned in the presence of flavins did not show any pitting in a window of −0.3- to +0.0-V overpotential in the bacterial medium. The results indicate that changes in the passive film chemistry induced by the presence of minute amounts of flavins during a mild anodic polarization can change the susceptibility of stainless steel surfaces to microbially influenced corrosion.

KEYWORDS

biofilms, flavins, MIC, microbially influenced corrosion, XANES

1 | INTRODUCTION

Austenitic stainless steels are widely used construction materials in various industrial applications due to their ability to provide corrosion resistance without compromising in strength.[1] Steels owe their corrosion resistance to the 1- to the 3-nm-thin protective passive film formed on the surface in contact with atmosphere. This passive film is governed by its chemical composition and electrochemical properties.[2,3] Despite the protective nature of the passive film, metal-reducing bacteria, like *Shewanella putrefaciens* CN32, can utilize iron and chromium species in the outermost oxide layer on the steel surface as an electron acceptor.[4–7] Thus, the chemistry and structure of the protective layer are altered, and microbiologically influenced corrosion (MIC) is responsible for changes in the corrosion resistance of stainless steels.[8,9] Iron is the most abundant transition metal in the environment, occurring mainly in two valence states as

oxidized ferric Fe(III) and reduced ferrous iron Fe(II). Iron-reducing microorganisms exhibit the ability to generate energy by coupling the reduction of Fe(III) to Fe(II) to the oxidation of organic matter.[10] In the context of MIC, the reduction of Fe(III)-containing oxides is expected to alter the stability of the passive film.

Alternatively to other modes of extracellular electron transfer (EET), *Shewanella* spp. can utilize self-secreted redox-active molecules for indirect electron transfer during their metabolic activity.[11–13] In the literature, it is described as the predominant mode, partially because the electron shuttle molecules, such as riboflavin (RB) and its derivative flavin mononucleotide (FMN),[14] are able to diffuse through the biofilm to the steel surface, overcoming large distances.[4] Moreover, flavin molecules are known to be able to act as chelating agents for iron oxides and to catalyze the cathodic oxygen reduction reaction.[4,15] It has been demonstrated recently (in Part I) that the presence of RB and FMN during mild anodic polarization results in thickening of the passive film with an increase in Fe(II) oxyhydroxides, leading to changes in the pit nucleation and corrosion properties.[16]

Xiao et al.[17] investigated whether riboflavin has the ability to inhibit ferrihydrite transformation. O'Loughlin[18] studied the effect of electron transfer mediators on the bioreduction of lepidocrocite by *S. putrefaciens* CN32. It was shown that the reduction of Fe(III) oxides by dissimilatory iron-reducing bacteria (DIRB) can result in the production of a suite of Fe(II) species including soluble Fe(II) complexes, Fe(II) complexes with organic and inorganic solid phases, and a wide range of mineral phases containing structural Fe (II) including magnetite (Fe_3O_4), siderite, or vivianite.[18] The analysis of the solid constituents by means of X-ray diffraction during Fe(II) production showed the gradual disappearance of lepidocrocite and concomitant formation of a carbonate green rust.[19,20] Green rusts are mixed ferrous/ferric hydroxides that have structures consisting of alternating positively charged hydroxide layers and hydrated anion layers, which have been reported as products of bioreduction of ferrihydrite and lepidocrocite by *S. putrefaciens* CN32.[18]

The role of iron-reducing bacteria in the microbiologically influenced corrosion (MIC) of steels is found to be inconclusive in the literature.[21,22] Recently, few studies have demonstrated that the oxygen scavenging effect of ferrous ions formed via the reductive dissolution of the Fe(III) oxyhydroxide-rich passive film by metal-reducing bacteria can inhibit corrosion processes on steels.[22–24] Additionally, the heterogeneous nature of the biofilm is another influencing factor determining the role of microorganisms in corrosion processes. Differential aeration cells can be formed beneath the biofilm, creating regions of cathodic and anodic character on the steel surface, which promotes corrosion processes.[23]

Miller et al.[24] demonstrated a protective effect of *Shewanella oneidensis* MR-1 on carbon steel when the biofilm is directly in contact with the metal surface. When a second biofilm-free surface is connected to that biofilm-covered surface over a zero resistance ammeter (ZRA), the corrosion of the uncovered surface is increased by 100%.[24] These findings are of significant importance for the understanding of MIC in technological systems, which are characterized by the presence of heterogeneous biofilms.

In this study, the exposure of stainless steel to flavins during a mild anodic polarization was studied with a focus on its effect on bacterial attachment, biofilm formation, and corrosion behavior on AISI 304 stainless steel. It aims to determine the influence of bacterial biofilm formation on the corrosion process and electrochemical behavior of the steel as well as the changes in the oxide chemistry. The ex-situ X-ray absorption near-edge structure (XANES) analysis was applied to investigate the corrosion products formed during incubation with *S. putrefaciens* on preconditioned stainless steel surfaces. The surface analysis was complemented by electrochemical and microscopic studies to characterize the differences in corrosion behavior. The results shall help to interpret the electrochemical interaction of bacteria with steels, especially regarding the indirect role of electron shuttle molecules in the corrosion behavior of microbial consortia.

2 | MATERIALS AND METHODS

2.1 | Sample preparation

Austenitic stainless steel sheets of type AISI 304 (1.4301, Goodfellow) were used as substrates. To achieve a comparable and reproducible passive film chemistry, all samples were electrochemically preconditioned at +50 mV versus sat. Ag/AgCl (three-electrode setup with a gold-wire counter electrode, Gamry 600+ potentiostat, C3 Prozessanalytik) in a noninteracting 20-mM $NaClO_4$ electrolyte with/without the addition of 1 μM of either RB or FMN. The comprehensive sample preparation and the detailed characterization of the substrates are reported elsewhere.[16]

2.2 | Cultivation of *S. putrefaciens* in a continuous culture

S. putrefaciens CN32 (ATCC® BAA-1097™), facultative anaerobic metal-reducing bacteria, were grown in continuous culture to eliminate cultivation-related influences of batch cultures. For this purpose, a chemostat was

TABLE 1 Composition of the *Shewanella* minimal medium (ShMM) (adapted from M9 minimal medium, Miller et al.[22])

ShMM (pH 7)	
NH_4Cl	15.0 mmol L^{-1}
Na_2SO_4	7.0 mmol L^{-1}
$MgSO_4$	0.4 mmol L^{-1}
$CaCl_2$	0.4 mmol L^{-1}
Na Glutamate	1.5 mmol L^{-1}
KH_2PO_4	4.25 mmol L^{-1}
Na_2HPO_4	4.25 mmol L^{-1}
Na Lactate	40 mmol L^{-1}

installed, providing the bacterial culture at a set absorbance at 600 nm (A_{600}) of 0.1 in late exponential growth state for all investigations. All settings were chosen on the basis of growth kinetics of CN32 in the minimal medium with an experimental growth curve investigation (plate count and absorbance monitoring over 3 days).

The chemostat is placed in a temperature-controlled water bath (30°C) on a magnetic stirrer and continuously aerated by purging a sterile stream of air through a porous glass filter placed at the bottom of the reactor. A feed solution of sterile *Shewanella* minimal medium (ShMM), pH 7 (Table 1, adapted from M9 minimal medium, Miller et al.[25]), with 40-mM lactate, is pumped at a flow rate of 10 ml/h. A drain prevents the culture flask from overflow and acts as a waste material outlet.

2.3 | Electrochemical methods

The prepared stainless steel samples were incubated with the bacterial culture at a 50:50 dilution with sterile ShMM, a minimal medium to set the bacteria into the exponential growth phase. During incubation, the biofilm formation was monitored by means of electrochemical impedance spectroscopy (EIS) over a period of 3 days. In a three-electrode setup, a saturated Ag/AgCl and a gold wire served as reference and counter electrodes, respectively. EIS spectra were collected in a frequency range of 100 MHz–10 MHz with an AC perturbation potential of 10 mV at a Gamry 600+ potentiostat (C3 Prozessanalytik). Over the whole incubation time, impedance scans were recorded every hour to follow the biofilm formation. Between the EIS data collection, the open-circuit potential (OCP) was monitored.

After 3 days of incubation, cyclic polarization measurements were performed in a potential range of −0.5 to +1.0 V versus OCP at a sweep rate of 1 mV/s with a current cutoff at 25 $\mu A/cm^2$. After the current cutoff was reached, the potential was cycled back with the same rate to the OCP value to investigate the repassivation behavior. All electrochemical tests were carried out at least as three independent measurements.

2.4 | Characterization of biofilm formation and MIC processes

After incubation and electrochemical studies, the samples were analyzed by means of scanning electron microscopy (SEM). No cyclic polarization scans were performed on preconditioned samples incubated only for biofilm analysis. These samples were washed by dipping in H_2O with stirring at 240 rpm for 20 s to remove nonadherent cell material. Fixation was peformed in a 2.5% glutaraldehyde solution for 4 h at 4°C (diluted 25% for electron microscopy; Merck), followed by washing in ddH_2O for 5 min and subsequent dehydration in an ethanol series (gradually increasing alcohol of 30%, 50%, 70%, 80%, 90%, and 100% [twice], each step for 15 min.) before imaging with an SEM. Here, an instrument of type Supra 40 (Zeiss) equipped with a Schottky field emitter was used, being operated at 1- and 10-kV accelerating voltage and using a conventional scanning electron (SE) and an additional SE-InLens detector. For the same sample systems, an independent replica was prepared and investigated by means of cyclic polarization. SEM imaging was performed after the removal of the biofilm at a Zeiss SEM EvoMA10 at 7×10^{-5} mbar operated at the 10-kV accelerating voltage in SE mode. For this purpose, the coupons were removed from the electrochemical cell, rinsed with deionized water, and cleaned in ethanol (98%, Sigma-Aldrich) in an ultrasonic bath for 10 min to remove the biofilms.

Surface chemistry characterization by means of XANES experiments has been performed at DELTA beamline 8.[26] A Si (111) double-crystal monochromator provided the energy intensity needed for studying the stainless steel compounds. Spectra were collected in the energy region of Fe K-edge (7112.8 eV), as well as Cr K-edge (5989.2 eV) within 60 eV below to 220 eV above the edge energies. In the XANES region, the data were collected at a 0.3-eV step size. Three consecutive gas-filled ionization chambers were applied as detectors. The samples under investigation (directly after preconditioning as well as after incubation with bacterial cultures or control media) were placed between the first and the second chamber, and a reference foil for exact energy calibration was placed between the second and third chamber. The beam spot size was adjusted to 80-μm height and 5-mm width. Steel coupons were prepared and incubated in bacterial culture onsite for 1 day. For sample alignment, a scan of the tilt angle θ was performed.[27] To reduce information from the bulk metal

and to be more sensitive to the surface thin film, the spectra of steel coupons were collected at grazing incidence with angles below the critical angle of the total reflection of the metal. The reference samples of different iron oxides and hydroxides were provided at the beamline and were measured in the transmission mode.[28–30]

The chromium is found in a deeper layer within the passive film, buried beneath the outermost iron oxide layers. Together with the growing biofilm, this results in a strong parasitic absorption at energies around the Cr K-edge. Therefore, the chromium spectra were not detected in the reflection mode, but in the fluorescence mode. A large area PIPS (passivated implanted planar silicon) fluorescence detector was placed in close vicinity parallel to the sample surface at 90° relative to the beam direction. The obtained spectra represent the ratio between the fluorescence detector signal to the signal of the incident photon beam from the first ionization chamber, employing an integration time of 4 s/eV step.

The IFEFFIT program package ATHENA (Demeter 0.9.26[31]) was used for pre/postedge correction. Calibration was set to 7112.8 eV of the maximum in the spectra's first derivative. By fitting the pre-edge and post-edge regions in the range of −60 to −8 eV and +35 to +150 eV, respectively, the relative K-shell contribution in the X-ray absorption spectra was obtained. The edge jump was adjusted to one for normalization. Each spectrum was collected three times consecutively to check the damage due to absorbed radiation and to improve the signal-to-noise ratio. All data presented are averages of measurements on three independent samples. As control measurements, steel coupons were also incubated with the supernatant of double-filtrated bacterial culture or dead-autoclaved bacterial culture. Two filters with 1.2- and 0.2-μm pore sizes, respectively, were used consecutively for preparing the filtrates.

3 | RESULTS

3.1 | Biofilm formation

After 3 days of incubation under electrochemical monitoring, the surface morphology of the biofilm-covered stainless steel specimen was fixated and analyzed by means of SEM. Biofilm growth was observed on all three sample systems, as seen in Figure 1. The coverage on stainless steel surfaces preconditioned in the presence of flavin molecules was higher than the surfaces preconditioned without the addition of flavins. Moreover, the samples preconditioned without flavins show a homogeneous coverage, whereas the biofilms formed on surfaces preconditioned in the presence of flavins are denser and patchier in terms of their structure. The dark areas representing the biofilm-covered surfaces show larger bacterial agglomerates with densely populated,

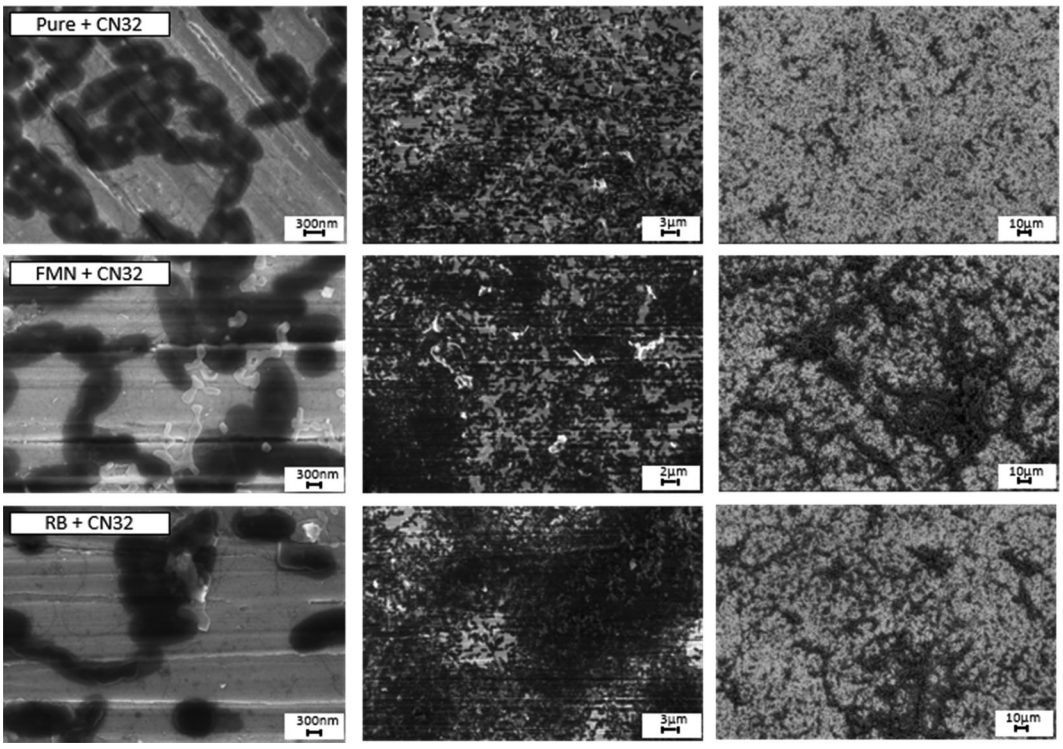

FIGURE 1 SEM micrographs of biofilm-covered stainless steel surfaces after fixation of the biomass; left and middle in InLens mode at 10 kV, right SE mode at 1 kV, 6-mm working distance. FMN, flavin mononucleotide; RB, riboflavin; SEM, scanning electron microscopy

three-dimensional structures and areas with less adhered cells. EIS was performed to investigate the biofilm growth and the changes with respect to the electrical properties of the passive film at the biofilm–stainless steel interface.

The heterogeneous structure of the biofilms, as indicated by the SEM analysis, necessitates the utilization of very complex equivalent circuits for the fitting of EIS spectra. Moreover, multiple equivalent circuits with up to three different constant phase element resistance couples have to be used to represent different phases of biofilm formation as well as oxide layer dissolution and growth. This results in a large parameter set and thus a high degree of freedom for the fitting process, which very often tends to converge in local minima with physically unsound values for individual elements. Therefore, EIS time traces are discussed qualitatively.

The contour maps presented in Figure 2 indicate that the main differences between the three substrates are observed within the first 12 h of incubation. The low-frequency impedance response provides information on the diffusion resistance of the growing biofilm, together with the charge transfer resistance due to initial changes in the passive film chemistry. The phase shift evolution is affected by both the double-layer capacitance and the biofilm capacitance in the low-frequency region. As seen in the contour map presented in Figure 2a, the low-frequency impedance of the sample preconditioned without the addition of flavins responds with an initial lag period of 6 h, followed by a continuous increase until reaching a plateau phase after 12 h. The same behavior can be observed in Figure 2b for the samples preconditioned in an FMN-containing electrolyte solution. Both systems reach similar impedance values, accounting for oxide growth with an increase in charge transfer resistance and biofilm coverage. For the sample preconditioned in an RB-containing electrolyte (Figure 2c), on the contrary, the impedance values initially decrease till 4.5 h, followed by a sharp increase during the next 2 h of incubation. The values leveled off after 9 h of incubation showing lower impedance values at the plateau level compared to the other two sample systems.

In the phase plots of Figures 2d–f, the flavin-preconditioned samples show at the beginning of incubation (0 h) a region of lower (more negative) angles in the frequency range of 0.1–1 Hz, visualized as dark green to blue range, which mainly contains the response of the oxide layer. The thickening of the oxide layer due to the preconditioning step in the presence of flavins was previously reported.[16] In presence of the bacteria, the pure steel samples show an oxide and biofilm growth with an increase in double-layer capacitance within 24 h of incubation after a phase of double-layer rearrangement in the first 6 h. The FMN sample does not exhibit a lag phase probably due to the high attractiveness of the surface for the bacteria and immediate settlement and

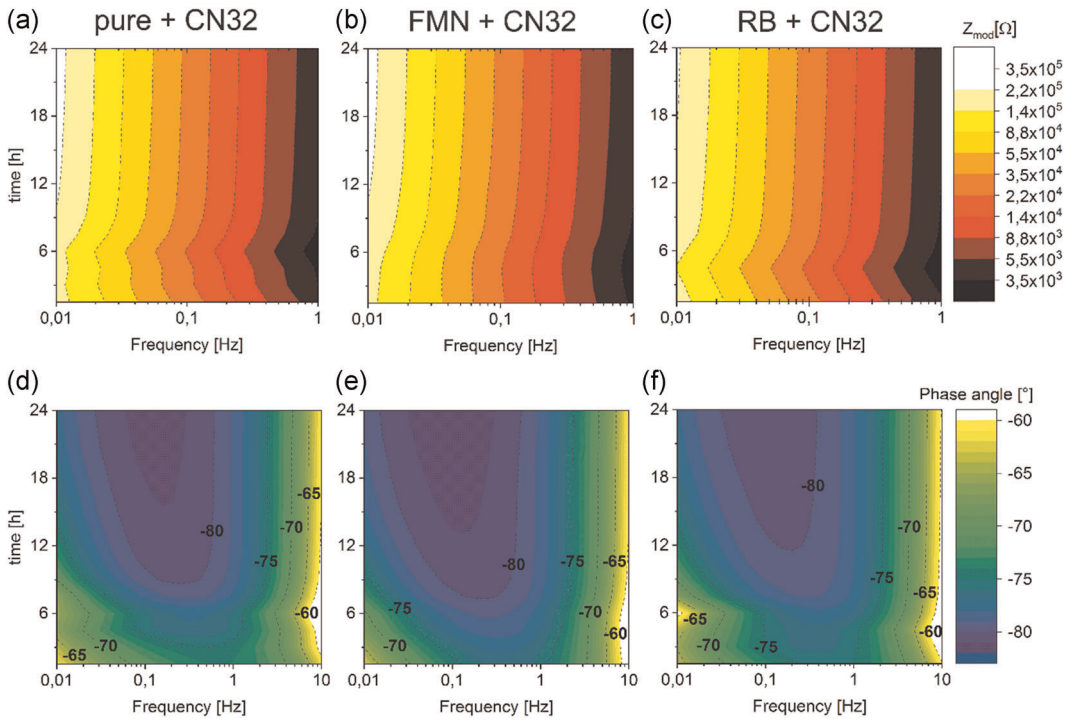

FIGURE 2 EIS spectra collected during the first day of incubation experiments, contour map representation of the low-frequency impedance (1 Hz to 10 MHz, a–c) and phase shift (10 Hz to 10 MHz, d–f). left to right: pure+CN32 (a,d); flavin mononucleotide (FMN) +CN32 (b,e), and RB+CN32 (c,f). EIS, electrochemical impedance spectrometry; FMN, flavin mononucleotide; RB, riboflavin [Color figure can be viewed at wileyonlinelibrary.com]

oxide growth. After 24 h of incubation, the FMN sample has the lowest values in the phase angle (highest negative values—darkest blue range) over a wide frequency region pointing toward a thickened oxide film and a homogenous biofilm coverage. However, the RB sample system at low frequencies responds with a loss of capacitive behavior at 6 h due to a patchy, three-dimensional biofilm growth with the presence of aeration channels/pores.

SEM images after the EIS cycles are shown in Figure 3. The RB sample did reveal an increased number of sites where micropitting was visible.

3.2 | Differences in the passive film chemistry

As presented in Part I, a detailed analysis of the surface chemistry and semiconducting properties has been performed by means of X-ray photoelectron spectroscopy (XPS) measurements and time-of-flight secondary ion mass spectrometry (ToF-SIMS) depth profiling before the incubation study to clarify the changes in the passive film chemistry and its effect on the corrosion properties. Briefly summarizing the results of Part I,[16] preconditioning in the presence of flavin molecules resulted in preferential growth of iron oxide/hydroxide-rich outer layers during passive film buildup.

Here in Part II, the focus of the investigations is on XANES spectroscopy and X-ray reflectivity measurements (pure, FMN, and RB, respectively) after incubation with the bacterial culture of *S. putrefaciens* CN32.

For sample alignment before the collection of grazing incidence XANES spectra, the angle between beam and sample surface was varied and the rocking scan of the tilt angle θ resulted in an angle-dependent reflectivity curve. In the literature, the reflectivity is used for the analysis of the thickness and interfacial roughness of multilayered thin-film samples.[32,33] The reflectivity signal is affected by the density of the materials in a layered film buildup.[34] Considering that the passive film on the stainless steel surface is less than 6 nm in thickness,[35–37] it can be expected that the measured reflectivity data will contain information from both surface film and the underlying metallic bulk material. Concerning this, the reflection curve will be an envelope of a peak at lower angles representing the lower density species as oxides and hydroxides and a higher angle component from the metallic species. In a recent study, we were able to demonstrate that reflectivity data can be used to obtain a first approximation of the changes in the passive film.[9]

The reflectivity data acquired on preconditioned samples before the incubation demonstrate the bilayer character of the passive film on the steel surface (Figure 4). At the Fe pre-edge energy (6900 eV), as seen in Figure 4a, the FMN and RB samples show a reflection peak and a critical angle that are shifted to lower angles with a greater FWHM (full width at half maximum), pointing to an increase in the species with lower density, and therefore a higher oxide or hydroxide content. The reflectivity peak measured at the Cr-edge energy (5800 eV, Figure 4b) is significantly broader than the one measured at the Fe edge, which can be explained by a broader distribution of chromium over the whole depth of the surface layer. As in the case of the Fe-edge reflectivity, both flavin systems have shown a similar trend in reflectivity scans at the Cr edge. For samples preconditioned without flavins, the reflectivity curve at the energy just below the Cr edge has a slight increase of the species at lower angles, which agrees very well with the surface analysis results regarding the preferential growth of an iron oxide/hydroxide-rich surface film and chromium depletion in the outermost region for both flavin systems.

As seen in Figure 4c,d, the reflectivity curve develops a defined second reflection peak at low θ-angles after incubation with bacteria. As sterile control, samples preconditioned without the addition of flavins (pure) were incubated with filtrated as well as autoclaved bacterial culture. The control measurements do not exhibit two separate features of the reflectivity peak. The evolution of a second peak at lower θ-angles can be explained by the thickening of the oxide/hydroxide surface film of lower density due to bacterial activity or the dissolution of ions from the steel surface that get trapped in the biofilm.

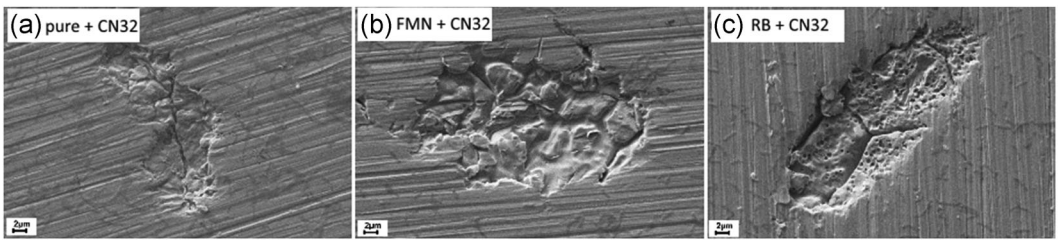

FIGURE 3 Pits found after incubation with bacteria with simultaneous EIS monitoring, SEM images in SE mode, EHT: 10 kV. EHT, electron high tension voltage; FMN, flavin mononucleotide; RB, riboflavin; SEM, scanning electron microscopy

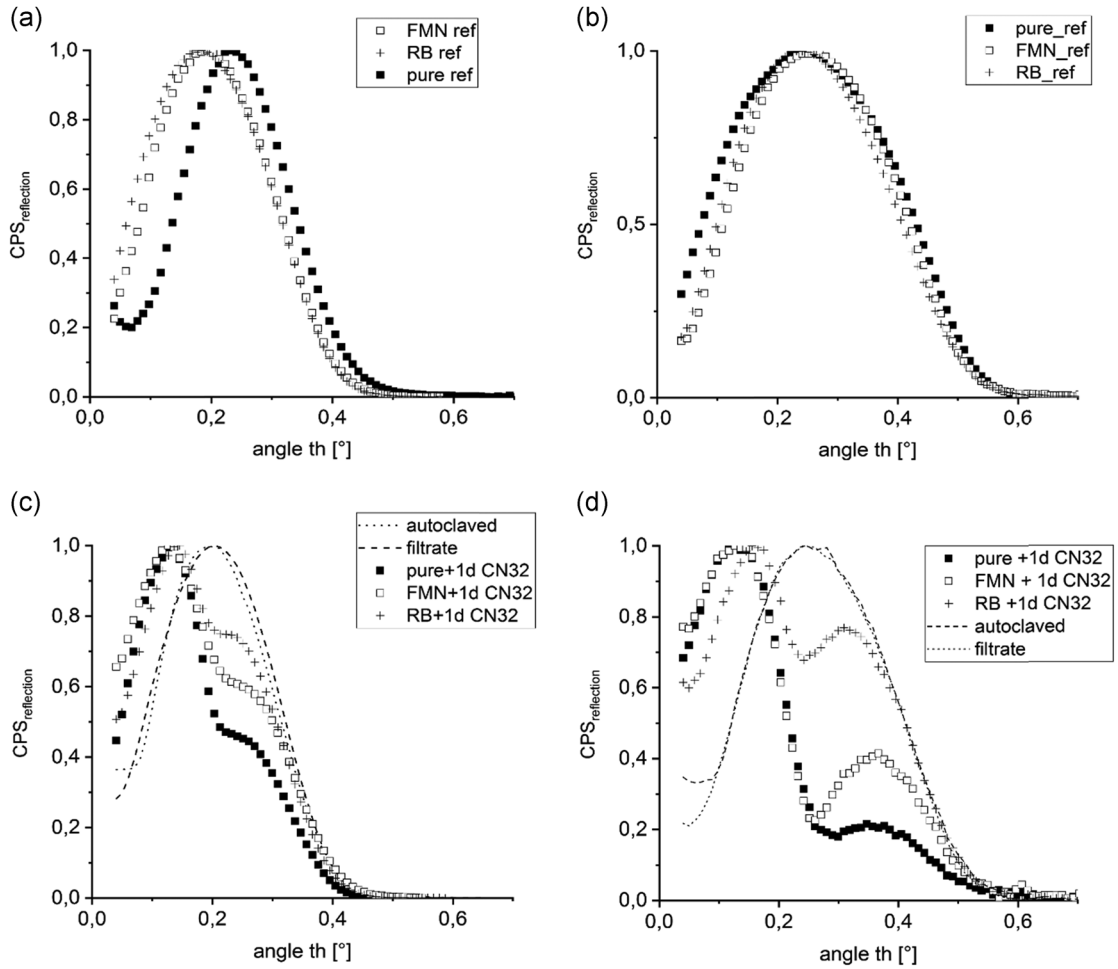

FIGURE 4 X-ray reflectivity scans on preconditioned surfaces before (a,b) and after incubation with bacteria (c,d), at energies just below Fe-edge energy (a, c) and Cr-edge energy (b,d), respectively. FMN, flavin mononucleotide; RB, riboflavin

The peak positions and separation can give insights into the thickness and the density of the surface oxides as well as the interfacial layer roughness.[32,33] The ratio between the low and high θ peaks in the reflection scan was calculated as 2.2 for pure+CN32, 1.7 for FMN +CN32, and 1.2 for RB+CN32, indicating that the growth of the lower density layer was in the following order: pure > FMN >> RB.

The XANES spectra are presented in Figure 5. As seen in Figure 5d, the preconditioning in the presence of FMN results in an increase of the iron oxides, especially Fe^{3+} species. Samples preconditioned in the presence of RB retain their oxide structure and show only a slight metallization.

After incubation, the metallic shoulder of the FMN sample is decreased and the oxide peak is increased in the energy range of Fe^{3+} oxides and hydroxides. A loss of iron (II) species can be observed. Incubation of the pure samples with bacteria led to a decrease in the metallic shoulder as well as an increase in the white line and a shift to higher energies. In contrast with the FMN sample, the Fe^{2+} signal was not lost completely with the pure sample. Overall, the changes are less pronounced for the pure sample, compared with the FMN sample. For the RB sample, on the contrary, the metallic shoulder, as well as the signal in the region of Fe^{2+} species, is slightly increased as compared with its preconditioning reference sample. This behavior is in contrast with both other sample systems.

The XANES spectra point out clear differences in the spectral contributions of the near-edge features. This can be observed in detail in the difference spectrum shown in Figure 5f. Due to the overwhelming signals from metallic bulk, the pre-edge region accounting for differences in oxide state is hidden. Only from the difference spectra, one can distinguish a negative change in the pre-peak intensity for FMN+CN32 samples, highlighting the loss of Fe^{2+} species. Moreover, the position of the absorption edge and the increased onset at around 7120 eV (inflection point), as well as the white line position (Figure 5g),

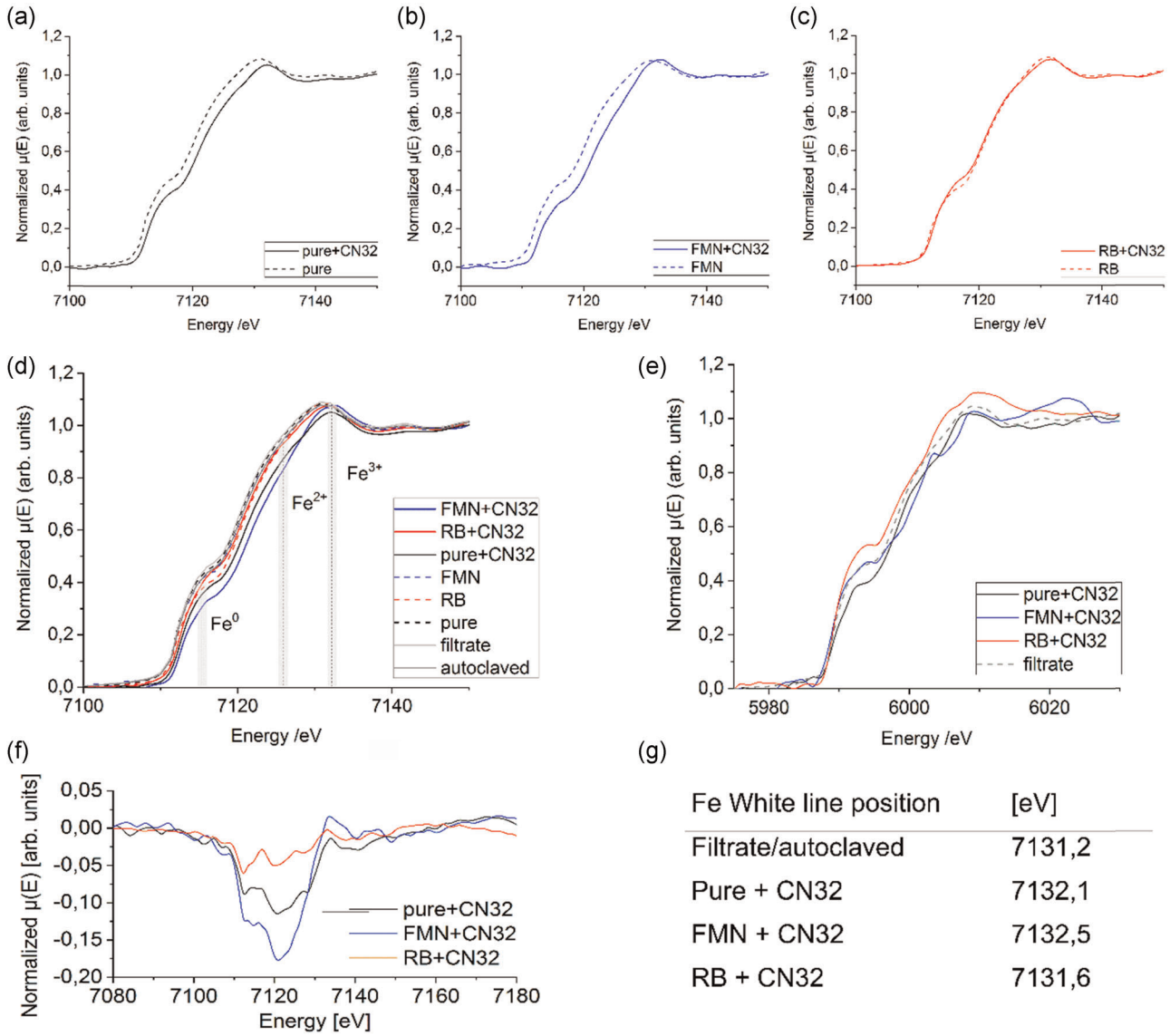

FIGURE 5 XANES spectra (average of three independent samples) on preconditioned steel substrates before and after incubation (1 day) in a bacterial culture at the Fe K-edge (a–c), (d) all samples after incubation in one graph, together with filtrate control measurement, (e) at the Cr K-edge energy; (f) difference XANES spectra at the Fe K-edge: Deviation from the control sample as curves and (g) shift of the white line position highlighted in the table. FMN, flavin mononucleotide; RB, riboflavin; XANES, X-ray absorption near-edge structure [Color figure can be viewed at wileyonlinelibrary.com]

are shifted to higher energies for the FMN+CN32 sample due to higher amounts of Fe^{3+} species. The difference spectra additionally reveal the significant increase of the oxide structure for the FMN+CN32 sample due to the sharp slope and the two intersects with the lines of the other systems. The RB+CN32 system, on the contrary, shows the lowest difference to the filtrate sample that was acting as a control.

The chromium K-edge spectra, presented in Figure 5e, indicates an increase of the metallic signal for the RB system as compared with the other substrates. The FMN+CN32 system shows some characteristics pointing to Cr_2O_3 and CrO_2 formation.[38]

3.3 | Corrosion properties

At the end of the 3-day incubation with EIS monitoring, cyclic polarization tests have been conducted and representative data of the resulting current density/potential curves are presented in Figure 6. To assure comparability, all measurements were performed in parallel with sterile control experiments. For the RB and FMN system incubated with bacteria, the repetitions of the corrosion potentials were very consistent with a deviation of less than 50 mV and negative hysteresis in the cathodic sweep. The pure system, on the contrary, showed significant differences in the pitting behavior

from measurement to measurement due to the lower and thinner biofilm coverage.

The first clear effect of the incubation with bacterial activity can be observed as a cathodic shift of OCP in the cyclic polarization results as compared with the control systems. This points to a corrosion inhibition effect as in an increased passive region ($E_{pit} - E_{corr}$ in Table 2). All samples incubated in the sterile control medium have shown a similar pitting behavior with pitting potentials between 0.56 and 0.87 mV (vs. sat. Ag/AgCl). The pure sample, after incubation with bacteria, did show pitting as well as a repassivation ability. The preconditioning in flavin-containing electrolytes resulted in a significant suppression of pitting after 3-day incubation in comparison to the samples preconditioned without flavins. Corrosion current (i_{corr}) values for samples incubated in CN32 cultures calculated by fitting the Tafel region of the forward anodic sweep were 0.2 $\mu A/cm^2$ for the pure system, 1.1 $\mu A/cm^2$ for the FMN sample, and 0.3 $\mu A/cm^2$, for the RB substrate. As listed in Table 2, a reduction of pit nucleation and prolonging of the passive region were also observed on substrates prepared in the presence of flavine molecules in abiotic corrosion experiments. This finding is supported by SEM images taken after the corrosion experiments. The control samples depicted in Figure 7 showed pit formation (see Part I[16] for a more detailed discussion). After incubation with bacterial culture, the pit form and size were different, as can be seen in Figure 8. The flavin-preconditioned samples after biofilm formation only showed a few small corrosion defects that appear only on the surface.

4 | DISCUSSION

The preconditioning of steel coupons in the absence or presence of flavin derivatives led to a preferential attachment and biofilm formation of *S. putrefaciens* CN32 on surfaces with an increased oxide thickness. The increase of species with a lower density in FMN and RB samples reported by a previous study[16] is supported by reflectivity data in this study. The increase of iron oxides/hydroxides due to the preconditioning step was accompanied by a lower donor density reported by Mott–Schottky analysis, previously.[16] This might have led to a higher dielectric constant that could be responsible for the easier biogenic iron reduction process to take place.[39] The utilization of iron as an electron acceptor is directly related to the electrical conductivity of the material. As the conductivity decreases with the increase in the film thickness as a result of defect annihilation, the flavine samples were prone to bacterial iron reduction. The incorporation or adsorption of FMN in/on the passive films, detected by means of ToF-SIMS analysis,[16] leads to a higher n-type character of the oxide layer before incubation. This redox-active molecule increases the electron transfer process and promotes the self-healing characteristic of the surface oxides.

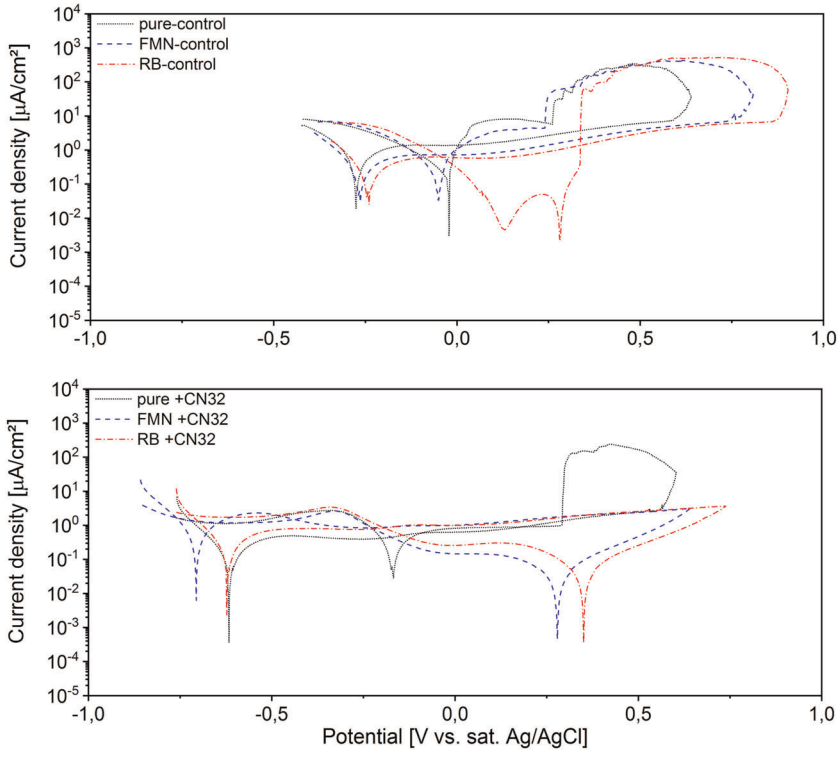

FIGURE 6 Representative cyclic polarization curves after 3 days of incubation with bacteria or sterile minimal growth medium as control measurements. FMN, flavin mononucleotide; RB, riboflavin [Color figure can be viewed at wileyonlinelibrary.com]

TABLE 2 Characteristics from cyclic polarization curves of stainless steel coupons after 3 days of incubation in either sterile ShMM (control) or in a bacterial culture

	Pure+CN32	FMN+CN32	RB+CN32	Pure control	FMN control	RB control
E_{corr} (V vs. Ag/AgCl)	−0.5	−0.70	−0.64	−0.25	−0.22	−0.2
E_{pit} (V vs. Ag/AgCl)	+0.62	–	–	+0.59	+0.75	+0.87
$E_{pit}-E_{corr}$ (V)	1.12	>1.5	>1.5	0.84	0.97	1.07

Abbreviations: FMN, flavin mononucleotide; RB, riboflavin; ShMM, *Shewanella* minimal medium

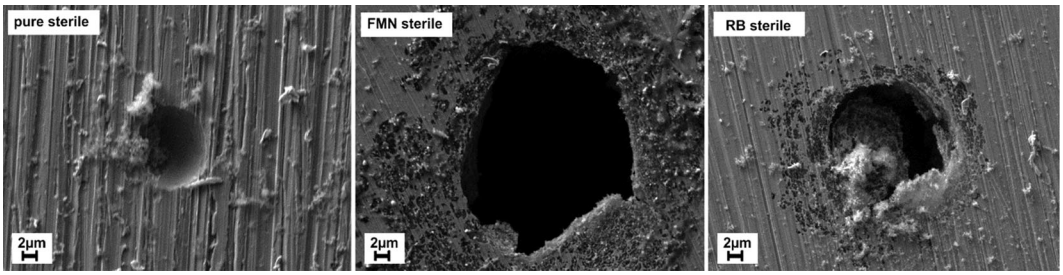

FIGURE 7 Pit formation on stainless steel substrates preconditioned in the presence and absence of biomolecules after 3 days of incubation in a bacterial culture after cyclic polarization experiments, EHT: 10 kV. (EHT, electron high tension voltage; FMN, flavin mononucleotide; RB, riboflavin

The reflection signals derived from grazing incidence X-rays are dependent on the refractive index of the material in the beam path. The peak position and separation in the reflectivity scans display that the RB system presents the thinnest oxide layer and the FMN sample presents the thickest after incubation with the bacterial culture. The RB sample, comparing the peak ratios in the θ scans of the iron and chromium energies, exhibits an increase of chromium distributed in the oxide layer. When considering that the chromium in the sample is buried under an iron oxide layer at the beginning of incubation experiments, the increase of chromium signal in the uppermost layers agrees well with the observation of Yuan and Pehkonen[40] concerning biofilms of

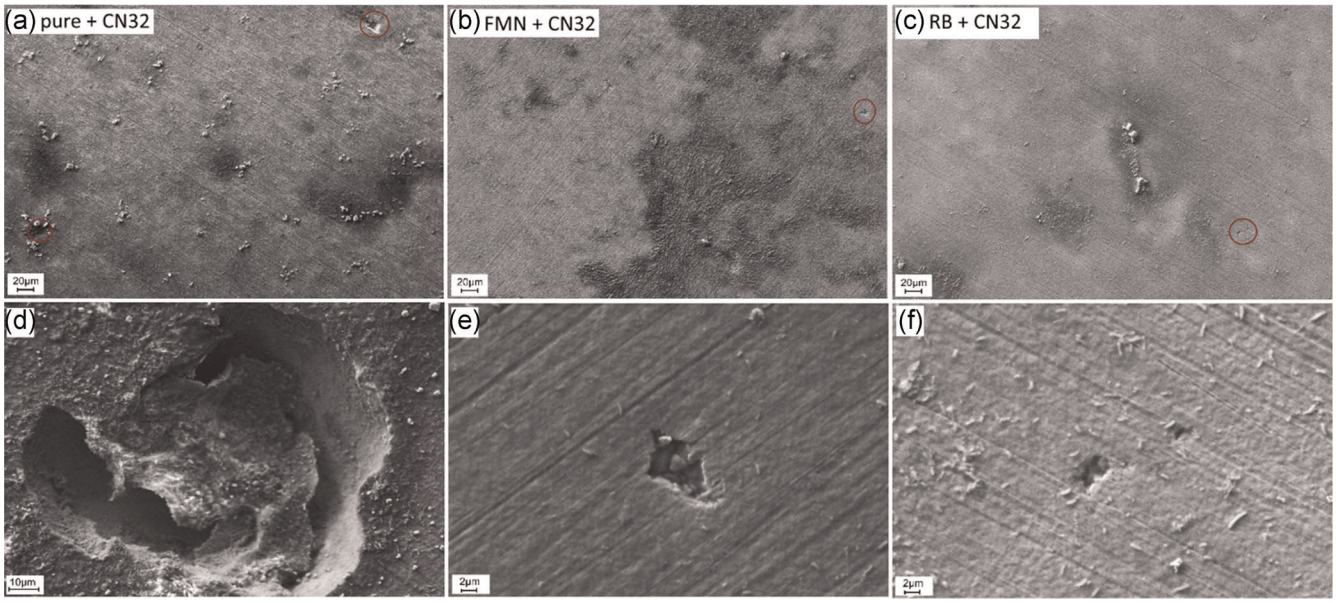

FIGURE 8 Pit formation on stainless steel substrates preconditioned in the presence and absence of biomolecules after 3 days of incubation in a bacterial culture after cyclic polarization experiments, EHT: 10 kV. EHT, electron high tension voltage; FMN, flavin mononucleotide; RB, riboflavin [Color figure can be viewed at wileyonlinelibrary.com]

Pseudomonas culture on AISI 304. Chromium is thought to accumulate in areas of iron depletion after the occurrence of localized corrosion as a result of extensive micro-pitting beneath the heterogeneous biofilm.[40–42] This phenomenon is visible in the SEM images presented in Figure 3. After incubation of prepared steel coupons in bacterial solution, samples of RB preconditioning also reveal micropitting phenomena inside the areas of the destroyed surface layer. The cyclic polarization experiments reveal that the flavin-preconditioned samples incubated in a sterile medium have already exhibited an inhibition effect emphasized by the delayed onset of pitting at higher anodic potentials. These results also indicate a higher general corrosion rate for the FMN samples, supporting the formation of the porous and less conductive oxide films at the biofilm–metal interface.

Additionally, the absence of pitting events in cyclic polarization diagrams after bacterial cultivation on the samples preconditioned in the presence of flavins can be explained by the fact that a thicker biofilm can act as a diffusion barrier. As presented in the study of Taillefert et al.,[43] the iron-reducing bacteria utilize amorphous Fe(III) faster than crystalline iron oxides. This means that the preconditioning step leading to a thicker and highly porous oxide/hydroxide structure for the RB sample[16] could have established optimum conditions for bacterial settlement and accelerated electrochemical activity with iron oxide depletion and micropitting events. For the RB system, incorporation or adsorption of the molecule on the stainless surface could not be detected by means of XPS, ToF-SIMS, or Fourier-transform infrared spectroscopy (data not shown). Therefore, it could be concluded that the changes in bacterial activity occur due to altered oxide chemistry. The Fe^{2+} shoulder in XANES data, especially in the RB sample, suggests that the Fe^{2+}-rich oxide film is stable during the incubation, which can act as a barrier and limit the iron(III) oxide reduction.[44] As reported by Roden and Urrutia,[45] the convective transport of Fe(II) could significantly influence the detection of microbial Fe(III) reduction. In contrast to the RB samples, adsorption or incorporation of FMN in the topmost layers was detected via the increased CN^- signal in the ToF-SIMS spectra.[16] The formation of such a monolayer of complexed phosphonogroups with the metal substrate might have led to the increased inhibition effect due to the M–O–P bonds, limiting the active surface area for bacterial attachment or electrochemical interaction.[38] The presence of FMN on the steel's surface after sample preparation could enable a direct pathway of electron shuttling between the surface and biofilm. These findings are consistent with the work of You et al.,[46] which revealed that not only the EET (extracellular electron transport) is accelerated but also biofilm thickness is enhanced in the presence of exogenic flavins. Similar to the work of Liu et al.,[47] a low biofilm coverage can increase MIC rates, and the lowest biofilm formation on the pure substrate caused the initiation of pitting corrosion during cyclic polarization experiments.

Overall, the results indicate that *S. putrefaciens* biofilms on AISI 304 stainless steel surfaces have a protective effect against pitting corrosion. This effect is enhanced when surfaces have been exposed to flavins, which were simulated in this study by a short-duration/low-magnitude anodic polarization in respective electrolytes.

5 | CONCLUSIONS

The effect of exposure to flavin-containing electrolytes on the biofilm formation of the iron-reducing microorganism *S. putrefaciens* and the resulting corrosion properties and microbial activity was investigated by means of XANES analysis and microscopic and electrochemical methods. Preconditioning in flavin-containing electrolytes promoted the biofilm formation. The analysis of X-ray reflectivity curves was used for an initial estimation of the changes in surface and interface chemistry. Interpreting the surface analysis presented in Part I,[16] together with XANES data collected on both the Cr and the Fe K-edges on samples after incubation experiments, it can be concluded that the enrichment of passive films in iron species during preconditioning in the presence of flavins resulted in an inhibition of pitting processes due to bacterial activity.

ACKNOWLEDGMENTS

Authors gratefully acknowledge the DELTA Synchrotron Facility for the assigned beamtimes and DELTA machine group (Dortmund) for providing synchrotron radiation reliably. Furthermore, they are very thankful to Sigrid Benemann (Federal Institute for Materials Research and Testing, Berlin, Germany) for the SEM images of the biofilms. Open access funding enabled and organized by Projekt DEAL.

CONFLICT OF INTERESTS

The authors declare that there are no conflict of interests.

AUTHOR CONTRIBUTIONS

Formal analysis, investigation, methodology, writing original draft, writing review, and editing: Nina Wurzler. *Investigation, writing review, and editing*: Jan D. Schutter and Vasile-Dan Hodoroaba. *Methodology, validation, writing review, and editing*: Ralph Wagner. *Methodology, writing review, and editing*: Matthias Dimper. *Methodology, supervision, writing review, and editing*: Dirk Lützenkirchen-Hecht. *Conceptualization, supervision, writing review, and editing*: Ozlem Ozcan.

DATA AVAILABILITY STATEMENT

The data that support the findings of this study are available from the corresponding author upon reasonable request.

ORCID

Ozlem Ozcan http://orcid.org/0000-0002-7457-4985

REFERENCES

[1] N. Aouina, F. Balbaud-Célérier, F. Huet, S. Joiret, H. Perrot, F. Rouillard, V. Vivier, *Electrochim. Acta* **2011**, *56*, 8589.
[2] C. O. A. Olsson, D. Landolt, *Electrochim. Acta* **2003**, *48*, 1093.
[3] J. J. de Damborenea, A. B. Cristobal, M. A. Arenas, V. Lopez, A. Conde, *Mater. Lett.* **2007**, *61*, 821.
[4] E. Marsili, D. B. Baron, I. D. Shikhare, D. Coursolle, J. A. Gralnick, D. R. Bond, *Proc. Natl. Acad. Sci. USA*. **2008**, *105*, 3968.
[5] J. K. Fredrickson, M. F. Romine, A. S. Beliaev, J. M. Auchtung, M. E. Driscoll, T. S. Gardner, K. H. Nealson, A. L. Osterman, G. Pinchuk, J. L. Reed, D. A. Rodionov, J. L. M. Rodrigues, D. A. Saffarini, M. H. Serres, A. M. Spormann, I. B. Zhulin, J. M. Tiedje, *Nat. Rev. Microbiol.* **2008**, *6*, 592.
[6] D. R. Lovley, *Curr. Opin. Biotechnol.* **2008**, *19*, 564.
[7] A. A. Carmona-Martinez, F. Harnisch, U. Kuhlicke, T. R. Neu, U. Schroder, *Bioelectrochemistry* **2013**, *93*, 23.
[8] H. A. Videla, L. K. Herrera, *Int. Microbiol.* **2005**, *8*, 169.
[9] N. Wurzler, J. D. Schutter, R. Wagner, M. Dimper, D. Lützenkirchen-Hecht, O. Ozcan, *Corr. Sci.* **2020**, *174*, 108855.
[10] A., Picard, D., Testemale, J.-L., Hazemann, I., Daniel, *Geochim. Cosmochim. Acta* **2012**, *88*, 120.
[11] Y. A. Gorby, S. Yanina, J. S. McLean, K. M. Rosso, D. Moyles, A. Dohnalkova, T. J. Beveridge, I. S. Chang, B. H. Kim, K. S. Kim, D. E. Culley, S. B. Reed, M. F. Romine, D. A. Saffarini, E. A. Hill, L. Shi, D. A. Elias, D. W. Kennedy, G. Pinchuk, K. Watanabe, S. Ishii, B. Logan, K. H. Nealson, J. K. Fredrickson, *Proc. Natl. Acad. Sci. USA* **2006**, *103*, 11358.
[12] C. R. Myers, J. M. Myers, *J. Bacteriol.* **1992**, *174*, 3429.
[13] A. Kappler, M. Benz, B. Schink, A. Brune, *FEMS Microbiol. Ecol.* **2004**, *47*, 85.
[14] R. Li, J. M. Tiedje, C. C. Chiu, R. M. Worden, *Environ. Sci. Technol.* **2012**, *46*, 2813.
[15] H. Liu, S. Matsuda, K. Hashimoto, S. Nakanishi, *ChemSusChem* **2012**, *5*, 1054.
[16] N. Wurzler, O. Sobol, K. Altmann, J. Radnik, O. Ozcan, *Mater. Corros.* **2021**, *72*.974.
[17] W. Xiao, A. M. Jones, X. Li, R. N. Collins, T. D. Waite, *Environ. Sci. Technol.* **2018**, *52*, 114.
[18] E. J. O'Loughlin, *Environ. Sci. Technol.* **2008**, *42*, 6876.
[19] M. Etique, F. P. A. Jorand, C. Ruby, *Geobiology* **2016**, *14*, 237.
[20] M. Stratmann, K. Hoffmann, *Corros. Sci.* **1989**, *29*, 1329.
[21] N., Kip, J. A. van Veen, *ISME J.* **2015**, *9*, 542.
[22] L. K. Herrera, H. A. Videla, *Int. Biodeter. Biodegr.* **2009**, *63*, 891.
[23] M. Dubiel, C. H. Hsu, C. C. Chien, F. Mansfeld, D. K. Newman, *Appl. Environ. Microbiol.* **2002**, *68*, 1440.
[24] R. B. Miller, A. Sadek, A. Rodriguez, M. Iannuzzi, C. Giai, J. M. Senko, C. N. Monty, *PLOS One* **2016**, *11*, e0147899.
[25] J. H. Miller, *Experiments in molecular genetics*, Cold Spring Harbor Laboratory, New York, NY **1972**.
[26] D. Lützenkirchen-Hecht, R. Wagner, U. Haake, A. Watenphul, R. Frahm, *J. Synchrotron. Rad.* **2009**, *16*, 264.
[27] D. Windover, D. L. Gil, Y. Azuma, T. Fujimoto, *Meas. Sci. Technol.* **2014**, *25*, 105007.
[28] D. Lützenkirchen-Hecht, L. Müller, L. Hoffmann, R. Wagner, *X-Ray Spectrom.* **2014**, *43*, 221.
[29] D. Lützenkirchen-Hecht, D. Wulff, R. Wagner, R. Frahm, U. Hollander, H. J. Maier, *J. Mater. Sci.* **2014**, *49*, 5454.
[30] N. Wurzler, J. D. Schutter, R. Wagner, M. Dimper, D. Lützenkirchen-Hecht, O. Ozcan, *Electrochem. Commun.* **2020**, *112*, 106673.
[31] B. Ravel, M. Newville, *J. Synchrotron. Rad.* **2005**, *12*, 537.
[32] D. Lützenkirchen-Hecht, M. Wagemaker, P. Keil, A. A. van Well, R. Frahm, *Surf. Sci.* **2003**, *538*, 10.
[33] J. Just, D. Lützenkirchen-Hecht, O. Müller, R. Frahm, T. Unold, *APL Mater.* **2017**, *5*, 126106.
[34] C. A. Helm, H. Möhwald, K. Kjaer, *J. Als-Nielsen Europhys. Lett.* **1987**, *4*, 697.
[35] L. Freire, M. A. Catarino, M. I. Godinho, M. J. Ferreira, M. G. S. Ferreira, A. M. P. Simoes, M. F. Montemor, *Cement Concrete Comp.* **2012**, *34*, 1075.
[36] A. Seyeux, S. Zanna, A. Allion, P. Marcus, *Corros. Sci.* **2015**, *91*, 352.
[37] J. J. Kim, Y. M. Young, *Int. J. Electrochem. Sci.* **2013**, *8*, 11847.
[38] S. Ould-Chikh, O. Proux, P. Afansiev, L. Khrouz, M. N. Hedhili, D. H. Anjum, M. Harb, C. Geantet, J.-M. Basset, E. Puzenat, *ChemSusChem* **2014**, *7*, 1361.
[39] A. Paszternák, I. Felhöse, Z. Pászti, E. Kuzmann, A. Vértes, E. Kálmán, L. Nyikos, *Electrochim. Acta* **2010**, *55*, 804.
[40] S. J. Yuan, S. O. Pehkonen, *Colloids Surf. B Biointerfaces* **2007**, *59*, 87.
[41] R. Gubner, I. B. Beech, *Biofouling* **2000**, *15*, 25.
[42] G. G. Geesey, R. J. Gillis, R. Avci, D. Daly, M. Hamilton, P. Shope, G. Harkin, *Corros. Sci.* **1996**, *38*, 73.
[43] M. Taillefert, J. S. Beckler, E. Carey, J. L. Burns, C. M. Fennessey, T. J. DiChristina, *J. Inorg. Biochem.* **2007**, *101*, 1760.
[44] E. E. Roden, J. M. Zachara, *Environ. Sci. Technol.* **1996**, *30*, 1618.
[45] E. E. Roden, M. M. Urrutia, *Environ. Sci. Technol.* **1999**, *33*, 1847.
[46] L.-X. You, L.-D. Liu, Y. Xiao, Y.-F. Dai, B.-L. Chen, Y.-X. Jiang, F. Zhao, *Bioelectrochemistry* **2018**, *119*, 196.
[47] H. Liu, T. Gu, M. Asif, G. Zhang, H. Liu, *Corros. Sci.* **2017**, *114*, 102.

SUPPORTING INFORMATION

Additional Supporting Information may be found online in the supporting information tab for this article.

How to cite this article: Wurzler N, Schutter JD, Wagner R, et al. Preconditioning of AISI 304 stainless steel surfaces in the presence of flavins—Part II: Effect on biofilm formation and microbially influenced corrosion processes. *Materials and Corrosion*. 2021; 72:983–994. https://doi.org/10.1002/maco.202012192